

University of Montana ScholarWorks at University of Montana

Numerical Terradynamic Simulation Group
Publications

Numerical Terradynamic Simulation Group

3-2018

Terrestrial primary production for the conterminous United States derived from Landsat 30 m and MODIS 250 m

Nathaniel P. Robinson

Brady W. Allred
University of Montana - Missoula

William P. Smith

Matthew O. Jones

Alvaro Moreno

See next page for additional authors

Let us know how access to this document benefits you.

Follow this and additional works at: https://scholarworks.umt.edu/ntsg_pubs

Recommended Citation

Robinson, Nathaniel P.; Allred, Brady W.; Smith, William P.; Jones, Matthew O.; Moreno, Alvaro; Erickson, Tyler A.; Naugle, David E.; and Running, Steven W., "Terrestrial primary production for the conterminous United States derived from Landsat 30 m and MODIS 250 m" (2018). *Numerical Terradynamic Simulation Group Publications*. 406.
https://scholarworks.umt.edu/ntsg_pubs/406


This Article is brought to you for free and open access by the Numerical Terradynamic Simulation Group at ScholarWorks at University of Montana. It has been accepted for inclusion in Numerical Terradynamic Simulation Group Publications by an authorized administrator of ScholarWorks at University of Montana. For more information, please contact scholarworks@mso.umt.edu.

Authors

Nathaniel P. Robinson, Brady W. Allred, William P. Smith, Matthew O. Jones, Alvaro Moreno, Tyler A. Erickson, David E. Naugle, and Steven W. Running

ORIGINAL RESEARCH

Terrestrial primary production for the conterminous United States derived from Landsat 30 m and MODIS 250 m

Nathaniel P. Robinson^{1,2} , Brady W. Allred^{1,2}, William K. Smith³, Matthew O. Jones^{1,2}, Alvaro Moreno², Tyler A. Erickson⁴, David E. Naugle¹ & Steven W. Running^{1,2}

¹W.A. Franke College of Forestry and Conservation, University of Montana, Missoula, Montana 59812, USA

²Numerical Terradynamic Simulation Group, University of Montana, Missoula, Montana 59812, USA

³School of Natural Resources and the Environment, University of Arizona, Tucson, Arizona 85721, USA

⁴Google, Inc., Mountain View, California 94043, USA

Keywords

Google earth engine, gross primary production, landsat, MOD17, MODIS, net primary production

Correspondence

Nathaniel P. Robinson, Numerical Terradynamic Simulation Group, University of Montana, Missoula, MT 59812.
Tel: +1 406 243 5521; Fax: +1 406 243 4510;
E-mail: nathaniel.robinson@umontana.edu

Funding Information

No funding information provided

Editor: Nathalie Pettorelli
Associate Editor: Jose Paruelo

Received: 7 September 2017; Revised: 12 January 2018; Accepted: 25 January 2018

doi: 10.1002/rse2.74

Remote Sensing in Ecology and Conservation 2018, **4** (3):264–280

Abstract

Terrestrial primary production is a fundamental ecological process and a crucial component in understanding the flow of energy through trophic levels. The global MODIS gross primary production (GPP) and net primary production (NPP) products (MOD17) are widely used for monitoring GPP and NPP at coarse resolutions across broad spatial extents. The coarse input datasets and global biome-level parameters, however, are well-known limitations to the applicability of the MOD17 product at finer scales. We addressed these limitations and created two improved products for the conterminous United States (CONUS) that capture the spatiotemporal variability in terrestrial production. The MOD17 algorithm was utilized with medium resolution land cover classifications and improved meteorological data specific to CONUS in order to produce: (a) Landsat derived 16-day GPP and annual NPP at 30 m resolution from 1986 to 2016 (GPP_{L30} and NPP_{L30} , respectively); and (b) MODIS derived 8-day GPP and annual NPP at 250 m resolution from 2001 to 2016 (GPP_{M250} and NPP_{M250} , respectively). Biome-specific input parameters were optimized based on eddy covariance flux tower-derived GPP data from the FLUXNET2015 database. We evaluated GPP_{L30} and GPP_{M250} products against the standard MODIS GPP product utilizing a select subset of representative flux tower sites, and found improvement across all land cover classes except croplands. We also found consistent interannual variability and trends across NPP_{L30} , NPP_{M250} , and the standard MODIS NPP product. We highlight the application potential of the production products, demonstrating their improved capacity for monitoring terrestrial production at higher levels of spatial detail across broad spatiotemporal scales.

Introduction

A primary process in all terrestrial ecosystems is the flux of carbon through trophic levels. Considered a supporting ecosystem service, primary production provides the foundation for numerous other services, including food, fuel, and fiber (Running et al. 2000; Haberl et al. 2007; Smith et al. 2012a). Terrestrial gross primary production (GPP) is the total amount of carbon captured by plants while net primary production (NPP) is the carbon allocated to

plant tissue after accounting for the costs of autotrophic respiration (Ruimy et al. 1994). GPP and NPP thus represent the carbon removed from the atmosphere and the carbon available to other trophic levels respectively (Field et al. 1995). The spatiotemporal variability in GPP and NPP across the terrestrial surface is substantial, and is primarily affected by climate, land cover, disturbance, and land use practices (Piao et al. 2009). Given the importance of GPP and NPP to ecosystem function and the capacity for humans to alter production via land use/land

cover change and climate change, developing appropriate products for monitoring these processes has emerged as a key component of ecological research, conservation, and management.

GPP and NPP cannot be directly observed at broad scales and requires models based on biophysical factors and atmospheric dynamics (Cramer et al. 1999; Scurlock et al. 1999). Models that integrate remotely sensed estimates of vegetation provide mechanisms for estimating, monitoring, and evaluating the spatiotemporal variability in terrestrial ecosystem production (Field et al. 1995; Running et al. 2000; Turner et al. 2004). One of the primary remote sensing-based models of terrestrial GPP and NPP is the Moderate Resolution Imaging Spectroradiometer (MODIS) MOD17 algorithm (Running et al. 2004; Sims et al. 2008; Smith et al. 2016). The MOD17 algorithm was originally designed for global monitoring and is widely applied across ecology (Haberl et al. 2007; Running 2012; Smith et al. 2012a,b; DeLucia et al. 2014). MOD17 products are currently the only regularly produced production products publicly available, with 8-day GPP and annual NPP estimates for the global vegetated surface at 1 km (version 5.5) and 500 m (version 6) spatial resolutions.

While the MOD17 product is widely utilized, trade-offs between temporal resolution, spatial resolution, and spatial extent restrict its use and applicability in ecology and natural resource conservation and management (Turner et al. 2003; Heinsch et al. 2006; Sims et al. 2008). Process based models like MOD17 are often computationally demanding and limited by computational processing and data storage capacity. To maintain global coverage, MOD17 inputs are spatially coarse, utilizing 0.5° (≈ 50 km) meteorological data, 500 m land cover classifications, and 500 m FPAR (fraction of photosynthetically active radiation), and LAI (leaf area index) estimates. The algorithm also relies on biome-specific parameters applied through a biome parameter look-up table (BPLUT). The BPLUT parameters are both parameterized and applied to biomes at the global scale, and thus do not capture variation within biomes (e.g., grasslands in North America use the same parameters as those in East Africa). While this simplification permits global estimations of terrestrial production, the coarse inputs and BPLUT approach attenuate ecologically important variation at finer scales (Running et al. 2000; Zhao et al. 2005; Neumann et al. 2016).

The patterns and spatiotemporal variability in GPP and NPP across landscapes are the result of numerous processes occurring at multiple spatiotemporal scales. Many of these processes occur simultaneously at fine resolutions but across broad spatial extents. Furthermore, human alteration and impact occurs at multiple scales. Discrete individual disturbances, small and potentially undetectable

in isolation, can have substantial impacts when viewed cumulatively (Allred et al. 2015). Land management activities (e.g., crop agriculture, grazing, or forestry) can occur at fine or broad spatial scales, as well as across long time periods. Due to its coarse resolution, the MOD17 product is generally ill-suited for evaluating production responses to finer-scale processes and impacts. To more effectively assess and monitor production, higher resolution products that balance the scales of observed patterns and underlying processes are needed.

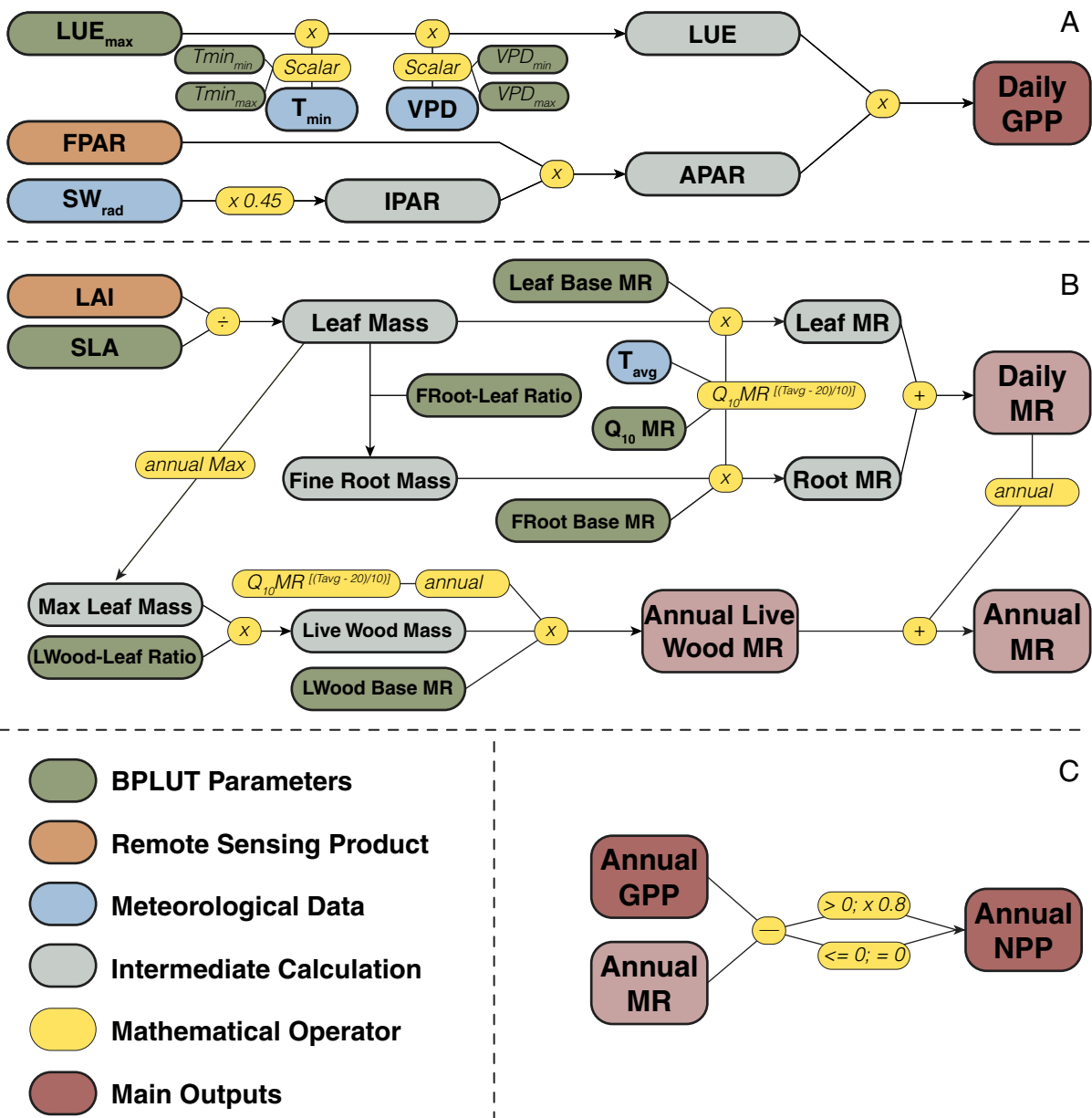
Addressing some of the limitations of the MOD17 product, we developed two separate medium resolution (30 m and 250 m) GPP and NPP products for the CONUS region. As the MOD17 algorithm is not bound to the coarse input datasets, we replaced input datasets with finer resolution and locally validated datasets, and optimized model parameters to reflect conditions specifically found within CONUS. We capitalized on advancements in cloud computing and parallel processing technologies to process historical Landsat and MODIS images alongside finer resolution meteorological data and land cover classifications to produce 30 m Landsat-derived GPP and NPP products from 1986 to 2016 (GPP_{L30} and NPP_{L30}) and 250 m MODIS-derived GPP and NPP products from 2001 to 2016 (GPP_{M250} and NPP_{M250}). We describe, evaluate, and emphasize the applicability of these two products, highlighting the capability to monitor terrestrial production at increased levels of spatial detail.

Materials and Methods

MOD17 overview

To create both the MODIS and Landsat derived production products we utilized the established framework of the MOD17 algorithm (Fig. 1). The theoretical basis for the MOD17 algorithm stems from original work by Monteith (1972), directly relating GPP and NPP to the amount of solar radiation absorbed by the plant canopy. Remotely sensed vegetation information was combined with light use efficiency logic and incident shortwave radiation to calculate daily GPP and after accounting for losses due to respiration, annual NPP.

The global input datasets of the MOD17 product were replaced with finer resolution datasets (Table 1). For the GPP/NPP_{M250} and GPP/NPP_{L30} products, we obtained meteorological inputs from the University of Idaho's 4-km gridded surface meteorological dataset, METDATA (Abatzoglou 2013). The meteorological inputs used to calculate light use efficiency and scale rates of respiration were short wave radiation, daily minimum and maximum temperature, and vapor pressure deficit. Land cover classifications from 1992, 2001, 2006, and 2011 were used to



Acronyms: LUE_{max} : maximum light use efficiency; LUE : light use efficiency; T_{min} : minimum daily temperature; VPD : daily vapor pressure deficit; $T_{min_{min}}$: minimum daily minimum temperature; $T_{min_{max}}$: maximum daily minimum temperature; VPD_{min} : minimum daily vapor pressure deficit; VPD_{max} : maximum daily vapor pressure deficit; SW_{rad} : short wave radiation; $FPAR$: fraction absorbed photosynthetically active radiation; $IPAR$: incident photosynthetically active radiation; $APAR$: absorbed photosynthetically active radiation; LAI : leaf area index; SLA : specific leaf area; MR : maintenance respiration; $FRoot$: fine root; $LWood$: live wood; T_{avg} : average daytime temperature

Figure 1. Flowchart of the MOD17 GPP and NPP algorithms. The main components are (A) GPP; (B) maintenance respiration; and (C) annual NPP. Adapted from the MOD17 user's guide (Running and Zhao 2015). NPP, net primary production; GPP, gross primary production.

Table 1. Underlying data sources for the MOD17 (500 m), MODIS derived GPP/NPP_{M250} (CONUS only; 250 m), and Landsat derived GPP/NPP_{L30} (CONUS only; 30 m) products. GPP, gross primary production; NPP, net primary production.

Input variable	Units	MOD17		MODIS250		LS30	
		Source	Resolution	Source	Resolution	Source	Resolution
VPD ¹	Pa	GMAO/NASA	0.5°	Idaho Metdata	4 km	Idaho Metdata	4 km
SWrad ²	w·m ⁻²	GMAO/NASA	0.5°	Idaho Metdata	4 km	Idaho Metdata	4 km
Tavg ³	°C	GMAO/NASA	0.5°	Idaho Metdata	4 km	Idaho Metdata	4 km
Tmin ⁴	°C	GMAO/NASA	0.5°	Idaho Metdata	4 km	Idaho Metdata	4 km
Land Cover	na	MOD12Q1	500 m	NLCD	30 m	NLCD	30 m
FPAR ⁵	na	MOD15A2	500 m	MOD09Q1	250 m	Landsat SR	30 m
LAI ⁶	m ² leaf m ⁻² ground	MOD15A2	500 m	MOD09Q1	250 m	Landsat SR	30 m

¹Vapor pressure deficit.

²Incident shortwave radiation.

³Average daytime temperature.

⁴Daily minimum temperature.

⁵Fraction of photosynthetically active radiation.

⁶Leaf area index.

apply biome-specific constraints throughout the algorithm, and were obtained from the 30 m National Land Cover Database (NLCD) (Homer et al. 2007, 2015; Fry et al. 2011). For GPP/NPP_{M250}, FPAR and LAI were calculated from the MODIS surface reflectance product, MOD09Q1 (Vermote 2015); for GPP/NPP_{L30}, FPAR and LAI were calculated from the Landsat surface reflectance products (Masek et al. 2006; Feng et al. 2012; Vermote et al. 2016). We used established relationships of FPAR and LAI with the normalized difference vegetation index (NDVI) (Choudhury 1987; Sellers et al. 1994; Peng et al. 2012; Wang et al. 2014).

As remotely sensed satellite data are inherently noisy due to atmospheric effects, cloud cover, data retrieval, and processing errors, a significant challenge is creating spatio-temporally continuous NDVI composites from which to calculate FPAR and LAI. The MOD09Q1 product is an 8-day global composite product that accounts for some of these underlying complexities. To account for temporal noise in the data, we smoothed data gaps and unusually low NDVI values based on the iterative Interpolation for Data Reconstruction (IDR) method (Julien and Sobrino 2010). Landsat data are more complex, due to an infrequent overpass interval, collection date differences between adjacent scenes, radiometric differences between missions, and various sensor malfunctions (e.g., Landsat 7 ETM+ scan line corrector error). Thus, we utilized a smoothing and climatology driven gap filling approach to create spatially continuous and temporal regular Landsat NDVI composites across CONUS (Robinson et al. 2017). Detailed descriptions of these methods are provided in the supporting information.

GPP

We used daily FPAR estimates, meteorological data, and the optimized parameter set to calculate daily GPP (eq. 1).

$$\text{GPP} = \text{LUE}_{\max} \times f_{T_{\min}} \times f_{\text{vpd}} \times 0.45 \times \text{SW}_{\text{rad}} \times \text{FPAR} \quad (1)$$

LUE_{\max} (g·C·MJ⁻¹) is a biome specific maximum potential light use efficiency and was attenuated by minimum temperature ($f_{T_{\min}}$) and vapor pressure deficit (f_{vpd}) scalars (Fig. S1) to account for temperature and water stress respectively. These scalars utilize other biome-specific properties ($T_{\min_{\min}}$, $T_{\min_{\max}}$, VPD_{\min} , and VPD_{\max}) to linearly scale the daily minimum temperature and daily vapor pressure deficit between 0 and 1. SW_{rad} (w·m⁻²) is incoming shortwave radiation, of which 45% is in wavelengths available for photosynthesis.

The original MOD17 BPLUT parameters represent global biomes and do not vary spatiotemporally. As the GPP products we developed are limited to CONUS, we optimized these parameters ($T_{\min_{\min}}$, $T_{\min_{\max}}$, VPD_{\min} , and VPD_{\max}) with reference GPP estimates from eddy covariance flux towers within CONUS. We used tier one level data from the FLUXNET2015 dataset, containing data from 43 tower sites across CONUS. To avoid the inclusion of poor quality data, we only used flux towers with at least 2 years of data and selected daily GPP observations flagged as high quality (quality flag ≥ 0.75) (Richardson et al., 2010; Verma et al., 2015). At some flux tower locations, there was a discrepancy in land cover as designated by the flux tower dataset and the dominant land cover as classified by the NLCD. To avoid flux towers in areas with heterogeneous land cover,

Table 2. The biome parameter lookup table (BPLUT) for MOD17, the GPP/NPP_{M250}, and the GPP/NPP_{L30}. GPP, gross primary production; NPP, net primary production.

Dataset	Parameter	ENF ¹	DBF ²	MF ³	SH ⁴	GR ⁵	CR ⁶
MOD17	LUE _{max}	0.00096	0.00117	0.00105	0.00128	0.00086	0.00104
	Tmin _{min}	-8.00	-6.00	-7.00	-8.00	-8.00	-8.00
	Tmin _{max}	8.31	9.94	9.50	8.61	12.02	12.02
	VPD _{min}	650.0	650.0	650.0	650.0	650.0	650.0
GPP/NPP _{M250}	VPD _{max}	4600.0	1650.0	2400.0	4700.0	5300.0	4300.0
	LUE _{max} ⁷	0.00132	0.00156	0.00144	0.00104	0.00142	0.00227
	Tmin _{min} ⁷	-9.43	-8.44	-8.94	-7.54	-10.56	-9.48
	Tmin _{max} ⁷	7.63	8.59	8.11	10.26	9.45	10.53
GPP/NPP _{L30}	VPD _{min} ⁷	721.51	745.26	733.39	627.08	778.52	723.69
	VPD _{max} ⁷	5703.33	3922.55	4812.94	4206.98	7040.36	5982.23
	LUE _{max} ⁷	0.00133	0.00142	0.00138	0.00101	0.00091	0.00176
	Tmin _{min} ⁷	-9.44	-8.15	-8.78	-7.94	-11.57	-10.31
All	Tmin _{max} ⁷	7.63	8.76	8.20	9.97	8.44	9.71
	VPD _{min} ⁷	722.23	733.84	728.04	647.37	828.54	765.33
	VPD _{max} ⁷	5714.47	3650.12	4682.30	4287.20	7697.52	6178.25
	LAI _{max} ⁸	6.501	6.091	6.296	6.328	6.606	6.543
	SLA	14.1	21.8	21.5	11.5	37.5	30
	Fine Root to Leaf Ratio	1.2	1.1	1.1	1.3	2.6	2
	Base Leaf MR	0.00604	0.00778	0.00778	0.00519	0.0098	0.0098
	Base Fine Root MR	0.00519	0.00519	0.00519	0.00519	0.00819	0.00819
	Q ₁₀ MR	2	2	2	2	2	2
	Live Wood to Leaf Ratio	0.182	0.203	0.203	0.04	0	0
Base Livewood MR	0.00397	0.00371	0.00371	0.00218	0	0	

¹Evergreen Needleleaf Forest.²Deciduous Broadleaf Forest.³Mixed Forest.⁴Shrubland.⁵Grassland.⁶Cropland.⁷Indicates parameters that were modified from the original MOD17 algorithm.⁸Indicates parameter added to the BPLUT for LAI calculations.

towers were only included if more than 50% of the pixels within a 1-km buffer were classified as the dominant land cover based on the NLCD and matched the given land cover classification of the flux tower. This resulted in 30 flux towers representing the range of land cover classes (Fig. S2; Table S1). Our optimization approach found the parameter set (Table 2) that minimized the residual sum of squares between model outputs and the corresponding flux tower GPP estimates for each land cover class (Turner et al. 2006, 2009). We utilized a limited memory, quasi-Newton algorithm (L-BFGS-B) for optimization (Byrd et al. 1995; Santaren et al. 2007), using original MOD17 BPLUT parameters as initialization values.

To validate the parameter optimization process, we implemented a cross-validation approach, whereby for each land cover, the data from each individual flux tower was iteratively withheld from the parameter optimization calculations. For each iteration, the resulting parameter set was used to predict daily GPP at the withheld tower

location. The predictions were assessed using the mean Pearson's correlation coefficients (r -values), root mean square error (RMSE), mean bias (MB), and mean absolute bias (MAB) as compared to daily flux tower GPP (GPP_{Flux}) for each land cover. These statistics were also calculated for GPP calculated with the original MOD17 parameters compared to GPP_{Flux}. Once the optimized parameter sets were obtained, differences between the datasets (GPP_{M250}, GPP_{L30}, MOD17 GPP) versus GPP_{Flux} were compared using r -values, RMSE, MB, and MAB. As the MOD17 product is an 8-day product, we matched GPP_{M250}, GPP_{L30}, and GPP_{Flux} to the temporal granularity of MOD17. Eight day periods with less than four valid flux tower observations were discarded.

NPP

Daily estimates of LAI, meteorological data, and the relevant MOD17 algorithm BPLUT parameters were used to

calculate daily maintenance respiration (MR). The logic and parameters were based on allometric relationships between estimated leaf area, leaf mass, fine root mass, and live wood mass. Annual NPP (eq. 2) was calculated as the sum of the daily differences between GPP and MR minus annual growth respiration (GR).

$$\text{NPP} = \sum_{i=\text{day } 1}^{365} (\text{GPP}_i - \text{MR}_i) - \text{GR} \quad (2)$$

To assess the quality of NPP_{M250} and NPP_{L30} estimates, we compared cumulative NPP, separated by land cover, across CONUS to the MOD17 product. Detailed methods for GPP and NPP are provided in the supporting information.

Products

GPP_{M250} is an 8-day cumulative estimate ($\text{kg}\cdot\text{C}\cdot\text{m}^{-2}\cdot 8\text{-days}^{-1}$) of GPP that matches the temporal resolution of the MOD17A2 GPP product; GPP_{L30} is a 16-day cumulative GPP estimate ($\text{kg}\cdot\text{C}\cdot\text{m}^{-2}\cdot 16\text{-days}^{-1}$). Both GPP products begin on day one of a given year and end on day 361 (MODIS derived 8-day) or 353 (Landsat derived 16-day). Each GPP composite includes the composite date and 7 or 15 ensuing days. The final period of each year is restricted to 5 days (6 days in a leap year) for GPP_{M250} and to 13 days (14 days in a leap year) for GPP_{L30} . The NPP_{M250} and NPP_{L30} are estimates of annual NPP ($\text{kg}\cdot\text{C}\cdot\text{m}^{-2}\cdot \text{year}^{-1}$). Data were scaled by 10,000 and stored as a 16-bit integer. Each of the products contain a QC band providing information regarding the underlying NDVI estimate for each pixel (Table 3). We utilized

Table 3. QC band pixel value descriptions for $\text{GPP}/\text{NPP}_{\text{M250}}$ and $\text{GPP}/\text{NPP}_{\text{L30}}$. GPP, gross primary production; NPP, net primary production.

Dataset	Pixel value	Description
GPP_{M250}	0	Original NDVI value used
	1	Smoothed NDVI value used
NPP_{M250}	0–100	Percent of NDVI values gap filled
GPP_{L30}	10	Clear not smoothed
	11	Clear smoothed
	20	Snow or water not smoothed
	21	Snow or water smoothed
	30	Climatology not smoothed
	31	Climatology smoothed
	40	Gap filled not smoothed
	41	Gap filled smoothed
	NPP_{L30}	0-100
255		Incomplete data (gap filling failed)

Differences in the QC values between the two products are due to different input datasets and processing methods. The pixel values indicate the quality of the NDVI values used in calculating FPAR and LAI.

Google Earth Engine (Gorelick et al. 2016) for data processing, product creation, and product distribution.

Results

GPP assessment

Evaluation of GPP calculated with the optimized cross-validated parameters compared to GPP with the original MOD17 algorithm parameter set yielded positive results for both GPP_{M250} and GPP_{L30} (Table 4). Across all flux tower sites combined, r -values increased from 0.60 to 0.79 (GPP_{M250}) and from 0.63 to 0.80 (GPP_{L30}), while RMSE values decreased from 4.33 to 2.83 (GPP_{M250}) and

Table 4. The Pearson's r -value, RMSE, bias, and mean absolute bias (MAB) among GPP_{M250} and GPP_{L30} and GPP_{Flux} . GPP, gross primary production; ENF, evergreen needleleaf forest; DBF, deciduous broadleaf forest; SH, shrubland; GR, grassland; CR, cropland.

Land cover	Tower vs. GPP_{M250}	Pearson's r	RMSE	Bias	MAB
All	Optimized parameters	0.79	2.83	0.02	1.72
	MOD17 parameters	0.60	4.33	1.90	2.42
ENF	Optimized parameters	0.83	1.67	0.26	1.27
	MOD17 parameters	0.82	2.20	1.59	1.73
DBF	Optimized parameters	0.89	2.67	0.26	1.27
	MOD17 parameters	0.57	5.15	3.21	3.48
SH	Optimized parameters	0.67	0.99	-0.07	0.70
	MOD17 parameters	0.72	1.23	-0.69	0.98
GR	Optimized parameters	0.75	1.85	-0.15	1.40
	MOD17 parameters	0.71	2.52	1.38	1.70
CR	Optimized parameters	0.71	4.94	-0.28	3.66
	MOD17 parameters	0.58	6.71	3.79	4.49

Land cover	Tower vs. GPP_{L30}	Pearson's r	RMSE	Bias	MAB
All	Optimized parameters	0.80	2.83	0.08	1.71
	MOD17 parameters	0.63	4.13	1.66	2.32
ENF	Optimized parameters	0.84	1.65	0.01	1.25
	MOD17 parameters	0.82	2.11	1.48	1.64
DBF	Optimized parameters	0.87	2.38	0.08	1.67
	MOD17 parameters	0.57	4.88	2.85	3.25
SH	Optimized parameters	0.66	1.05	0.08	0.74
	MOD17 parameters	0.69	1.33	-0.76	1.07
GR	Optimized parameters	0.72	2.01	0.39	1.46
	MOD17 parameters	0.69	2.29	1.00	1.58
CR	Optimized parameters	0.66	5.00	0.14	3.74
	MOD17 parameters	0.55	6.39	3.28	4.35

Results are mean values for each landcover of the iterative cross-validation approach, and include GPP calculated with both the original MOD17 algorithm parameters and optimized parameters produced in this paper. The optimized parameters for both datasets yielded better statistics across all land cover classes except shrublands Pearson's r value.

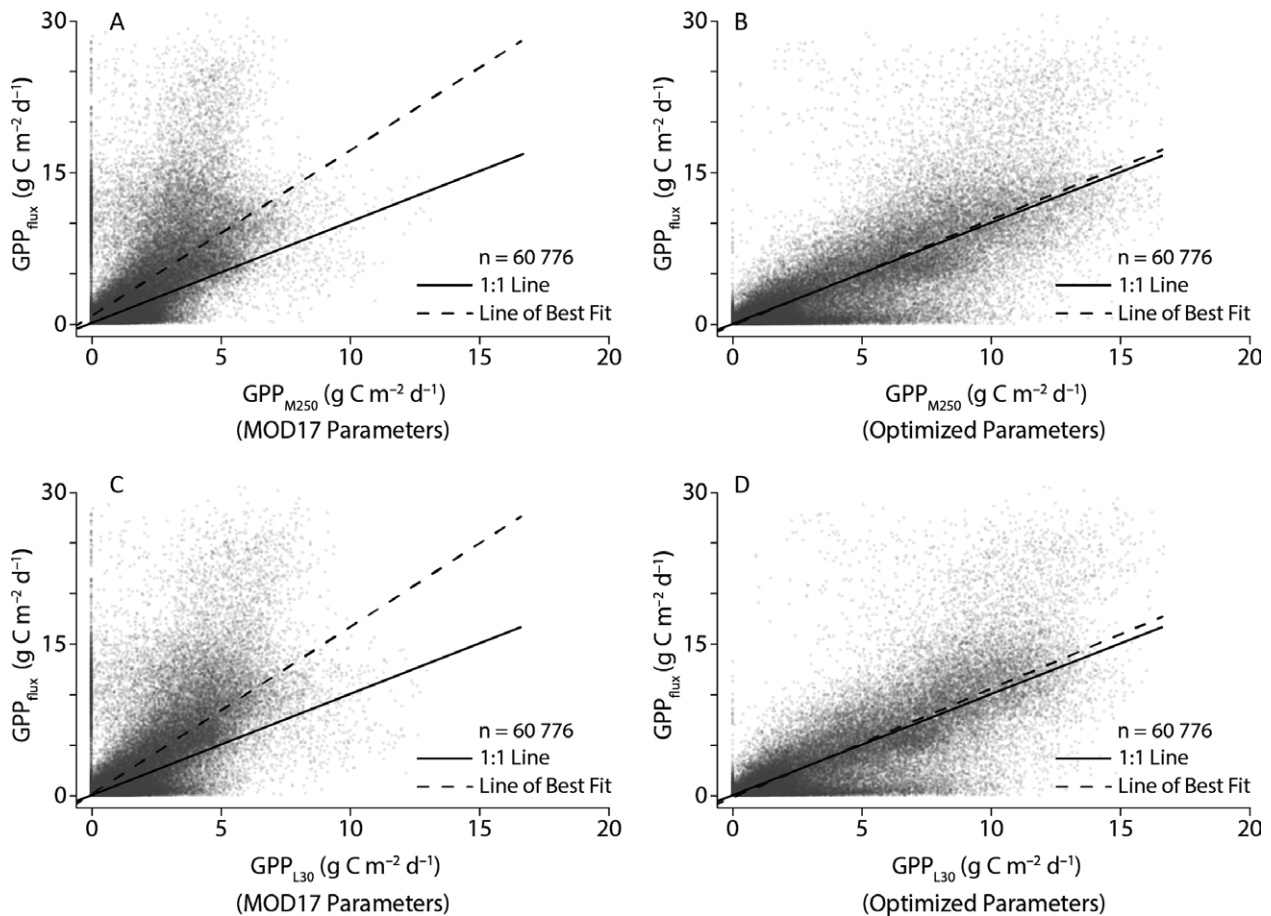


Figure 2. GPP_{M250} (A & B) and GPP_{L30} (C & D) relative to GPP_{Flux} (FLUXNET2015, CONUS only). GPP₂₅₀ GPP_{L30} in plots A and C are calculated with the original MOD17 BPLUT parameters, while GPP in B and D use parameters optimized for CONUS. GPP, gross primary production.

from 4.13 to 2.83 (GPP_{L30}). Incorporating the optimized parameters linearized the relationship between the modeled estimates of GPP and GPP_{Flux} (Fig. 2). Analysis of flux towers aggregated by land cover also produced improved results for most land cover classes (Fig. 3; Table 4). Deciduous broadleaf (DBF) sites improved the most with r -values increasing from 0.57 to 0.89 (GPP_{M250}) and from 0.57 to 0.87 (GPP_{L30}) and RMSE decreasing from 5.15 to 2.67 (GPP_{M250}) from 4.88 to 2.38 (GPP_{L30}). Shrubland (SH) sites revealed little change with optimized parameter sets, with decreases in RMSE values from 1.23 to 0.99 (GPP_{M250}) and from 1.33 to 1.05 (GPP_{L30}) and decreases in r -values from 0.72 to 0.67 (GPP_{M250}) and from 0.69 to 0.66 (GPP_{L30}). Of the six shrubland sites, five (44 of 46 site-years) were in semi-arid regions of Arizona and Utah. The shrubland class constituted a diverse functional group, and this diversity was poorly represented in this clustering. Eddy covariance flux measurements in semi-arid areas often include significant components of abiotic CO₂ fluxes, which may result

in the overestimation of GPP_{Flux} using traditional flux partitioning procedures (Serrano-Ortiz et al. 2014).

When comparing to GPP_{Flux}, both GPP_{M250} and GPP_{L30} showed improvements over MOD17 GPP across all land cover classes except cropland (Table 5). Excluding croplands, the r -values improved from 0.91 (MOD17) to 0.94 (GPP_{M250}) and 0.93 (GPP_{L30}), while the RMSE decreased from 1.49 (MOD17) to 1.29 (GPP_{M250}) and 1.31 (GPP_{L30}). Seasonally, the temporal profiles of modeled GPP tracked the profiles of flux tower GPP (Fig. 4). Across most flux towers, GPP_{M250} and GPP_{L30} corresponded more closely to GPP_{Flux} than the MOD17 product GPP. The most notable discrepancies were in cropland sites, where all models tend to underestimate peak flux tower GPP (Fig. 4D). The poor performance of MOD17 within croplands is well-documented and improved methods are needed to capture the wide variation in parameters across crop types (Chen et al. 2011) and nonlinearities between LUE and GPP within croplands (Guanter et al. 2014; Wood et al. 2017).

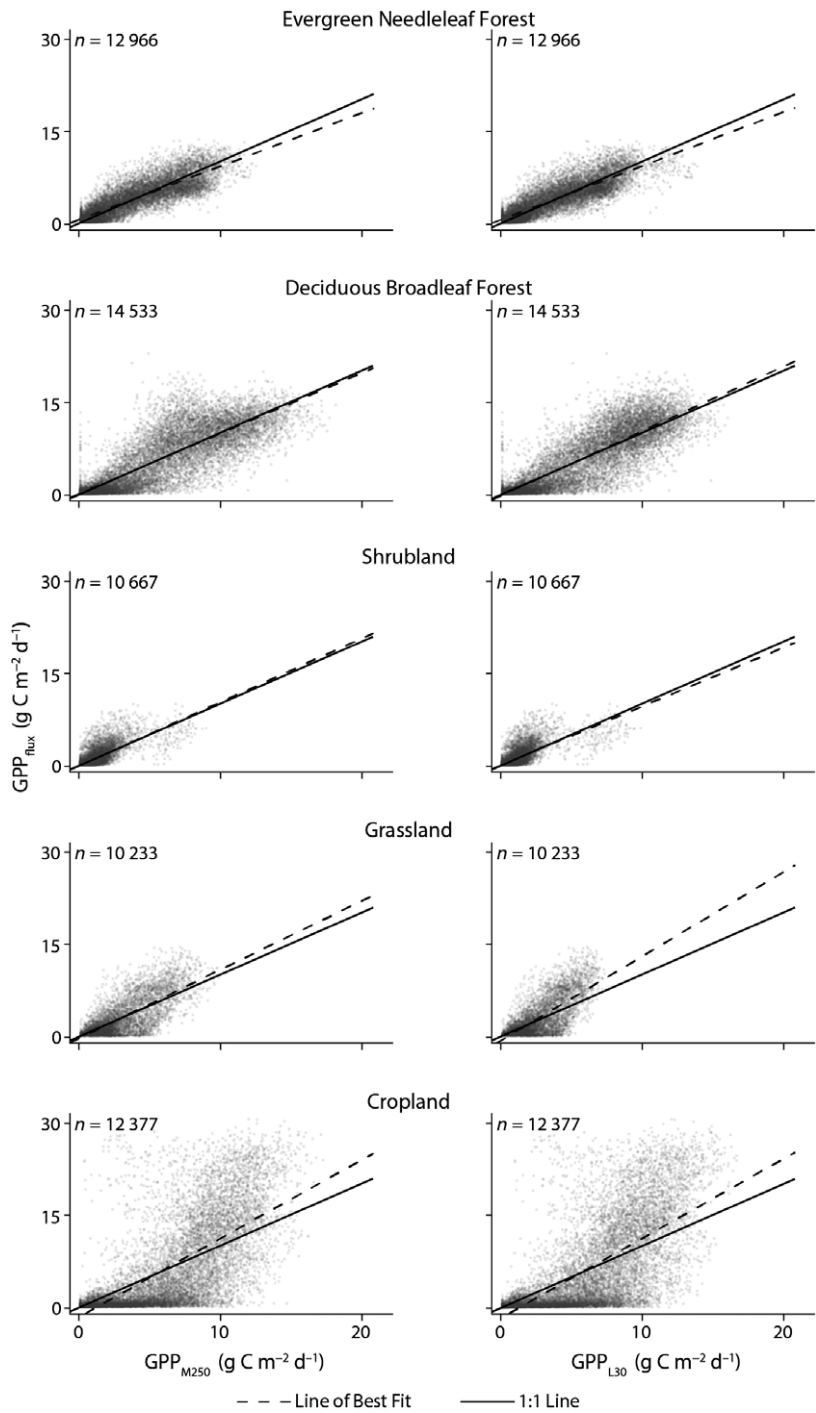


Figure 3. GPP_{M250} (left column) and GPP_{L30} (right column) relative to GPP_{Flux} (FLUXNET2015, CONUS only), aggregated by land cover. GPP, gross primary production.

NPP assessment

Comparing total annual NPP across CONUS (Table 6), we found high correlations between both NPP_{M250} and NPP_{L30} relative to the MOD17 product (NPP_{M250} r -value: 0.82; NPP_{L30} r -value: 0.81). From 2001 to 2014, average annual NPP from the MOD17 product was estimated at

3.09 petagrams (Pg; 10^{15} g) of carbon while for the NPP_{M250} NPP_{L30} it is 4.49 Pg and 3.03 Pg respectively. When compared to the MOD17 product, NPP_{M250} was 41–50% higher, while NPP_{L30} was 1.7–2.0% lower. The relatively high NPP_{M250} estimates were largely caused by differences in the parameterization of LUE_{max} for croplands (Table 2). While comparing the total absolute

Table 5. Pearson's r -value, RMSE, bias and mean absolute bias (MAB) between flux tower GPP and the MOD17 product, GPP_{M250} and GPP_{L30}. GPP, gross primary production; ENF, evergreen needleleaf forest; DBF, deciduous broadleaf forest; SH, shrubland; GR, grassland; CR, cropland.

Tower	Dataset	Pearson's r	RMSE	Bias	MAB
All	MOD17	0.89	1.53	0.09	0.96
	GPP _{M250}	0.91	1.55	-0.48	1.02
	GPP _{L30}	0.90	1.50	-0.26	0.99
ENF	MOD17	0.90	1.07	-0.33	0.72
	GPP _{M250}	0.93	1.09	-0.32	0.76
	GPP _{L30}	0.94	0.90	-0.19	0.62
DBF	MOD17	0.91	1.98	-0.12	1.28
	GPP _{M250}	0.95	1.62	-0.55	1.12
	GPP _{L30}	0.94	1.70	-0.09	1.13
SH	MOD17	0.69	1.04	0.03	0.68
	GPP _{M250}	0.76	0.94	0.04	0.62
	GPP _{L30}	0.74	0.97	0.04	0.64
GR	MOD17	0.63	1.30	0.13	0.78
	GPP _{M250}	0.69	1.23	-0.27	0.84
	GPP _{L30}	0.66	1.28	-0.25	0.86
CR	MOD17	0.68	1.82	0.24	1.25
	GPP _{M250}	0.66	2.86	-1.84	2.15
	GPP _{L30}	0.65	2.57	-1.53	1.96

These comparisons use 8-day mean GPP, matching the temporal granularity of the MOD17 product. Bold indicates the best statistic.

values of NPP across a region is useful for general validation purposes, discrepancies between models are expected due to the utilization of different input datasets and parameterization. More informative is the degree to which each product tracks interannual variability in total NPP. We found consistent interannual variability and seasonal magnitudes across all three NPP products for all land cover classes (Fig. 5). The only notable exception occurred in the shrubland class (SH), where NPP_{L30} shows higher deviations from the mean in 2004 and 2012. NPP_{M250} and NPP_{L30} consistently underestimated NPP across shrublands compared to the MOD17 product, likely originating from an underestimation of GPP (see GPP Assessment) or an overestimation of respiration (see Strengths, Challenges, and the Future).

Discussion

We produced 30 m and 250 m GPP and NPP products for CONUS that better capture the spatiotemporal variability in terrestrial production than currently available coarser resolution products (Fig. 6). Accounting for this variability reveals changes in production dynamics, particularly important for smaller scale monitoring, conservation, and land management (Fig. 7; see also cased studies and figures in Supporting Information). By optimizing the parameters with GPP data from FLUXNET2015 towers located within

CONUS and using improved land cover and climate data specific to CONUS, we further refine the algorithm to more accurately reflect regionally unique conditions.

Value for conservation and management

Remotely sensed GPP and NPP extend satellite imagery beyond commonly used vegetation indices or land cover change. Production, measured in units of carbon, allows for assessing ecosystem dynamics in ecological, economical, and socially relevant terms (Vitousek et al. 1986; Haberl et al. 2004; Crabtree et al. 2009). Better understanding—specifically with improved spatial resolution—of how land use activities affect carbon dynamics is critical in an era where climate change poses a massive challenge. Production also provides a foundation for process based models used to estimate ecosystem services, such as cropland agriculture (McGuire et al. 2001; Monfreda et al. 2008), forest stand biomass (Keeling and Phillips 2007; Hasenauer et al. 2012), or rangeland forage (Hunt and Miyake 2006; Reeves et al. 2006). As many land use activities that can alter these and other ecosystem services occur at finer scales across landscapes, medium, and high-resolution products are necessary for assessment and monitoring. For example, while the rapid energy development across the United States is a major driver of land use change (McDonald et al. 2009; Trainor et al. 2016), the cumulative impacts of these developments, specifically on terrestrial production, has been difficult to assess due to the broad geographic extent and the scale mismatch between the disturbances and products (Allred et al. 2015). Coarser resolution NPP products fail to detect discrete losses in NPP caused by disturbance at finer scales (Fig. 7). The NPP_{L30} product improves the tracking and accounting of these discrete losses while also extending the historical record. Built into decision frameworks, production information can help managers better understand the dynamics, impacts, and trade-offs of their management (see also Supporting Information, *Applications* section and Fig. S4 and S5). Quantifying conservation outcomes, e.g., management practices, restoration activities, etc., at fine resolutions, across broad spatial extents, and in relevant ecological terms (biomass, carbon), is essential in evaluation and adaptive management.

Strengths, challenges, and the future

The Landsat (30 m) and MODIS (250 m) derived products have specific applications they are best suited for. The finer resolution of Landsat sensors allows for more detailed examination of production dynamics and responses to human activities that are largely absent in coarser products. The historical Landsat archive adds

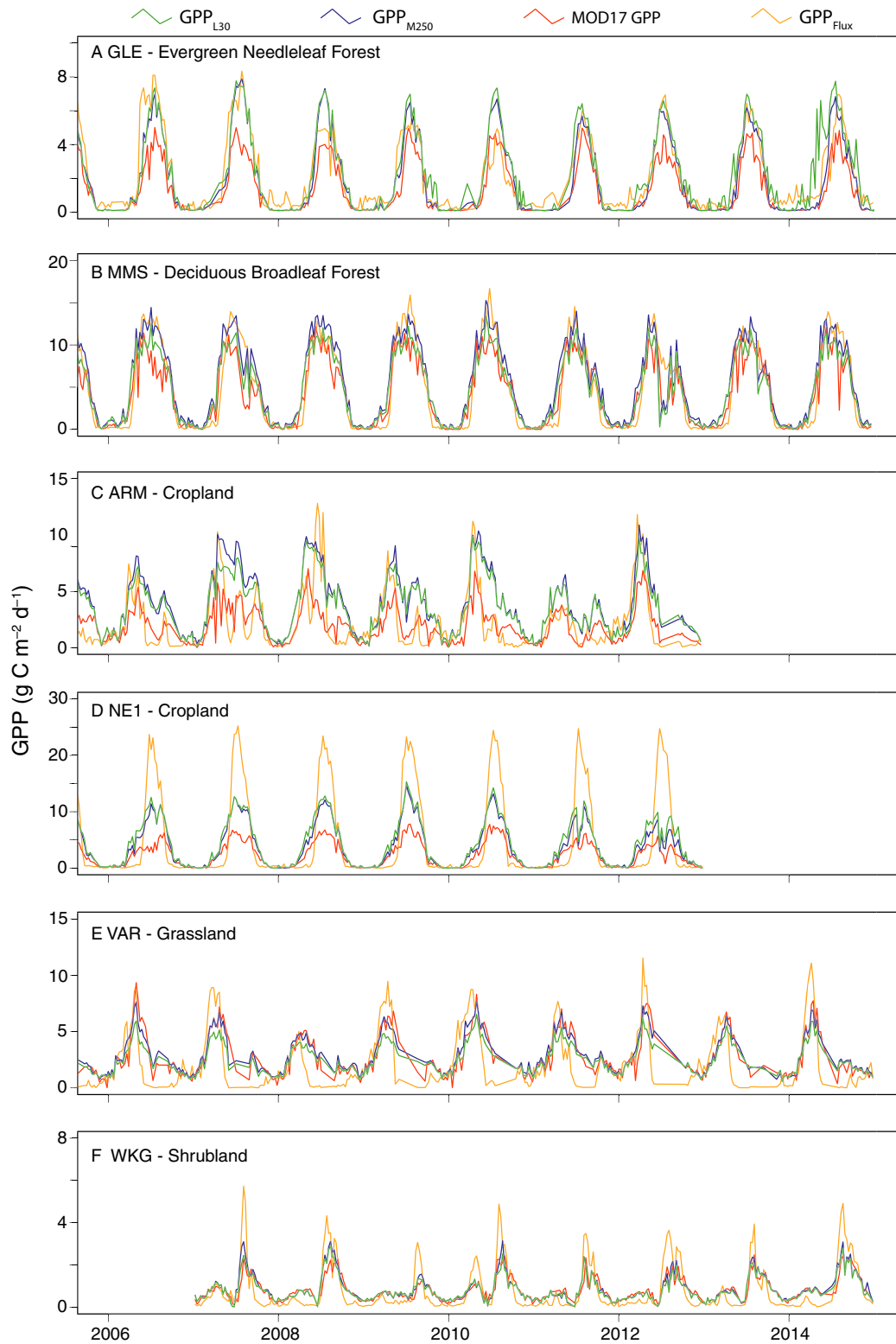


Figure 4. Time series of 8-day GPP_{Flux} , MOD17 GPP (500 m), GPP_{M250} (250 m) and GPP_{L30} (30 m) from towers representing the range of land cover classes. Data from two cropland towers (C and D) are plotted demonstrating the range of GPP variability across cropland sites. The GPP_{M250} and GPP_{L30} datasets correspond well with GPP_{Flux} at the ARM flux tower (C; Oklahoma, wheat and soybean) while underestimate GPP compared to GPP_{Flux} at the NE1 flux tower (D; Nebraska, irrigated corn). GPP, gross primary production.

Table 6. Total annual NPP for CONUS in Pg (10^{15} g) carbon for MOD17, NPP_{M250}, and NPP_{L30}. NPP, net primary production; ENF, evergreen needleleaf forest; DBF, deciduous broadleaf forest; MF, mixed forest; SH, shrubland; GR, grassland; CR, cropland.

Land cover	Product	2001	2002	2003	2004	2005	2006	2007	2008	2009	2010	2011	2012	2013	2014	Mean
Total	MOD17	2.996	2.946	3.275	3.389	3.217	2.880	3.196	3.162	3.137	3.297	2.880	2.786	3.070	3.120	3.097
	NPP _{M250}	4.606	4.192	4.762	5.017	4.712	4.504	4.699	4.631	4.692	4.617	3.864	3.892	4.069	4.566	4.487
	NPP _{L30}	3.114	2.834	3.221	3.431	3.194	3.054	3.139	3.208	3.267	3.137	2.519	2.491	2.712	3.148	3.034
ENF	MOD17	0.606	0.543	0.609	0.629	0.644	0.573	0.565	0.585	0.595	0.605	0.519	0.508	0.570	0.607	0.583
	NPP _{M250}	0.657	0.588	0.635	0.681	0.661	0.639	0.635	0.615	0.645	0.612	0.535	0.561	0.575	0.636	0.620
	NPP _{L30}	0.616	0.556	0.598	0.638	0.625	0.602	0.593	0.594	0.613	0.588	0.503	0.525	0.534	0.604	0.585
DBF	MOD17	0.602	0.634	0.752	0.710	0.630	0.565	0.578	0.654	0.661	0.651	0.613	0.614	0.683	0.631	0.641
	NPP _{M250}	0.923	0.837	0.987	1.000	0.889	0.907	0.886	0.929	0.926	0.861	0.752	0.779	0.799	0.886	0.883
	NPP _{L30}	0.701	0.630	0.758	0.772	0.672	0.675	0.637	0.715	0.720	0.649	0.509	0.501	0.573	0.675	0.656
MF	MOD17	0.093	0.089	0.096	0.101	0.091	0.087	0.087	0.092	0.091	0.091	0.087	0.087	0.091	0.089	0.091
	NPP _{M250}	0.125	0.113	0.123	0.127	0.120	0.120	0.115	0.117	0.118	0.114	0.103	0.111	0.106	0.115	0.116
	NPP _{L30}	0.153	0.138	0.152	0.156	0.147	0.146	0.139	0.145	0.146	0.138	0.119	0.129	0.127	0.143	0.141
SH	MOD17	0.378	0.366	0.404	0.441	0.456	0.396	0.459	0.407	0.394	0.457	0.380	0.384	0.393	0.414	0.409
	NPP _{M250}	0.257	0.235	0.270	0.317	0.317	0.261	0.295	0.263	0.281	0.297	0.234	0.222	0.242	0.279	0.269
	NPP _{L30}	0.179	0.162	0.187	0.237	0.224	0.179	0.211	0.186	0.204	0.204	0.149	0.127	0.158	0.191	0.186
GR - Natural	MOD17	0.334	0.315	0.358	0.382	0.384	0.325	0.435	0.360	0.361	0.402	0.325	0.292	0.337	0.369	0.356
	NPP _{M250}	0.604	0.527	0.621	0.660	0.650	0.561	0.676	0.612	0.635	0.663	0.523	0.502	0.549	0.623	0.600
	NPP _{L30}	0.309	0.274	0.317	0.343	0.336	0.295	0.346	0.329	0.344	0.351	0.351	0.266	0.273	0.332	0.319
GR - Pasture/ Hay	MOD17	0.379	0.387	0.410	0.414	0.377	0.345	0.393	0.394	0.377	0.401	0.351	0.363	0.373	0.368	0.381
	NPP _{M250}	0.552	0.508	0.576	0.591	0.544	0.535	0.542	0.556	0.545	0.535	0.457	0.484	0.482	0.535	0.532
	NPP _{L30}	0.232	0.211	0.244	0.251	0.229	0.227	0.227	0.241	0.235	0.224	0.184	0.191	0.196	0.292	0.227
CR	MOD17	0.597	0.606	0.638	0.705	0.628	0.583	0.672	0.663	0.650	0.683	0.599	0.532	0.616	0.635	0.629
	NPP _{M250}	1.488	1.384	1.550	1.642	1.532	1.480	1.577	1.540	1.543	1.537	1.260	1.235	1.317	1.493	1.470
	NPP _{L30}	0.925	0.863	0.965	1.032	0.961	0.930	0.985	0.998	1.103	0.983	0.783	0.751	0.836	0.975	0.935

Results are shown aggregated across all land cover as well for each class individually.

another 15+ years to that available with MODIS, permitting longer trend analysis. Landsat derived production (GPP_{L30} and NPP_{L30}) is best suited for detailed, smaller scale assessments where responses or trends of localized areas are desired. The 16-day return interval of satellites and temporal offset between adjacent orbital paths, however, can create discontinuous data across broad scales. Although the compositing and gap filling mitigates much of the resulting effects and artifacts, they do not eliminate them. The daily overpass of MODIS sensors make MODIS derived estimates of production well-suited for analysis across broad geographic regions or continental analysis. MODIS derived production (GPP_{M250} and NPP_{M250}) minimizes atmospheric and cloud contamination; increases resolution from 500 to 250 m relative to the MOD17 product, permitting examination of some of the finer scale processes and responses (Fig. 6); and follows the same 8-day schedule of the MOD17 product. Users should examine both products before application to determine which is appropriate for their needs.

Despite the noted improvements and added utility of the high-resolution products, some of the simplifying assumptions and limitations of the MOD17 algorithm itself are maintained in our methods. First, there is an

unmeasured propagation of errors, stemming from the underlying accuracy and mismatched resolution of input datasets. Second, the biome specific parameters do not vary spatiotemporally and are applied through temporally discrete land cover datasets, which may not reflect rapid land cover change. Third, the optimization process is based on a limited and clustered network of flux tower data. While users should be aware of these limitations, these are key areas for future research and product development. For example, strategies to incorporate the spatiotemporal variability in key parameters or to more accurately represent land cover through time at sub-pixel levels are promising approaches for improvement (Madani et al. 2014; Yang et al. 2015). Additionally, respiration is a key source of uncertainty in the NPP algorithm (Fig. 1B), as it is calculated independently from GPP and utilizes biome level allometric relationships (Turner et al. 2005; Zhang et al. 2009). Simplifying respiration to a fixed proportion of GPP can avoid associated uncertainties (DeLucia et al. 2007; Zhang et al. 2009; Van Oijen et al. 2010). A fixed ratio reduces the interannual variability in NPP across land cover classes and removes the NPP anomalies in shrublands and deciduous forest (Fig. S6, Table S3).

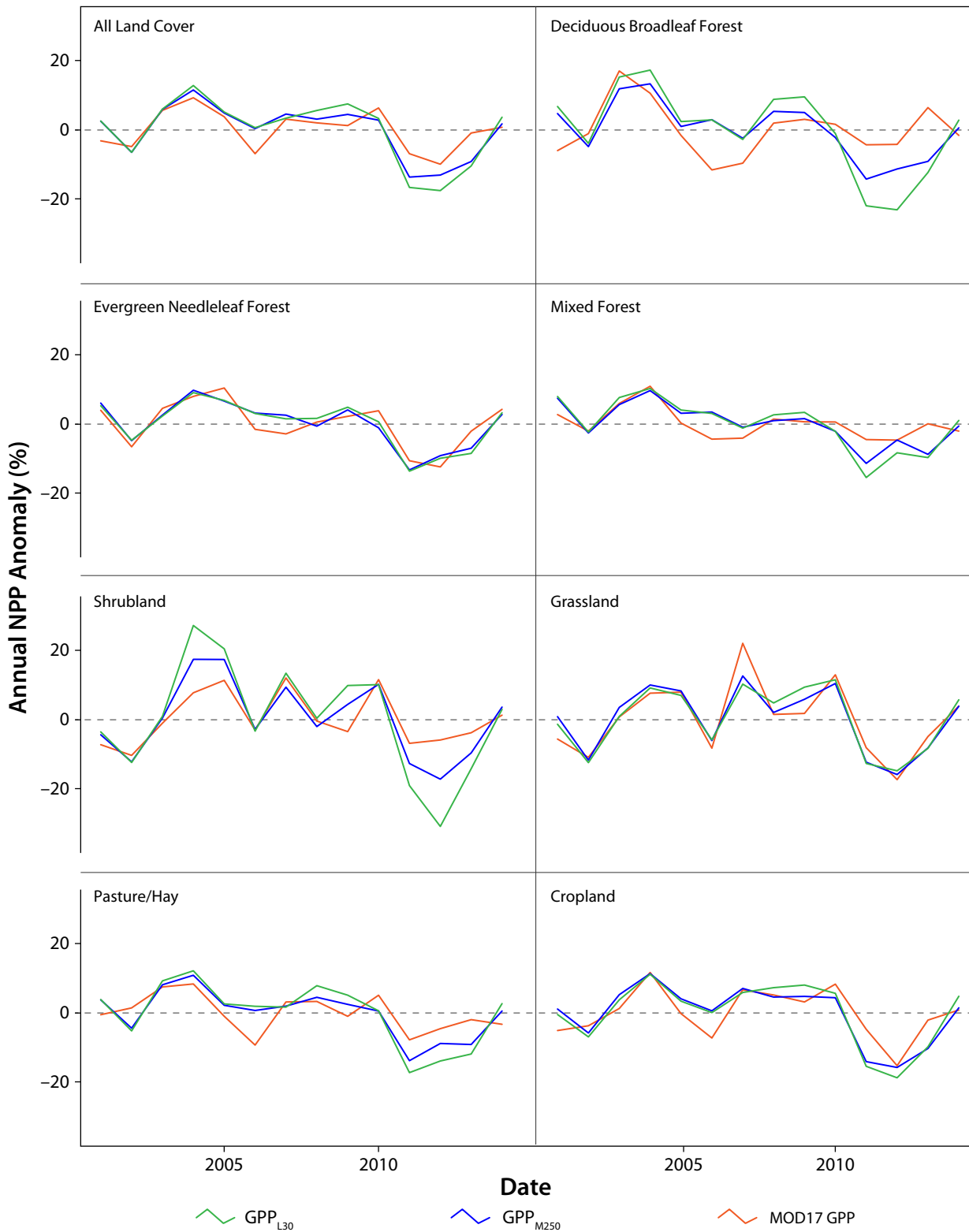


Figure 5. Time series of NPP anomalies for the MOD17 (500 m), NPP_{M250} (250 m), and NPP_{L30} (30 m) datasets. All three datasets track the interannual variability of NPP with similar magnitudes. Anomalies are calculated as the percent difference from the long-term mean for each dataset and land cover class. NPP, net primary production, GPP, gross primary production.

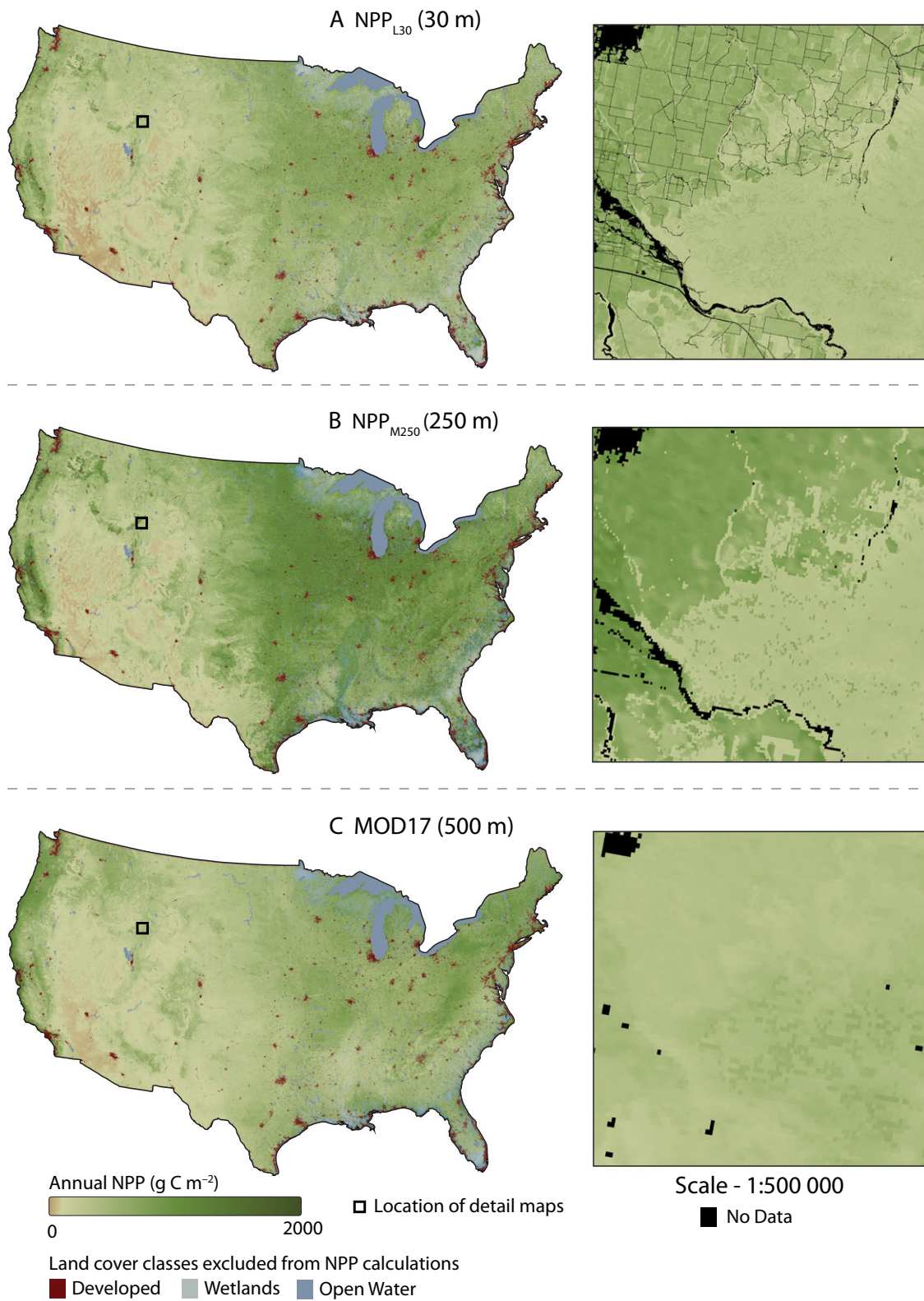


Figure 6. Maps of 2010 annual NPP across CONUS at levels of decreasing resolution: (A) NPP_{L30} at 30 m; (B) NPP_{M250} at 250 m; and (C) the MOD17 product at 500 m. Higher resolution reveals greater spatial variability of NPP. NPP, net primary production.

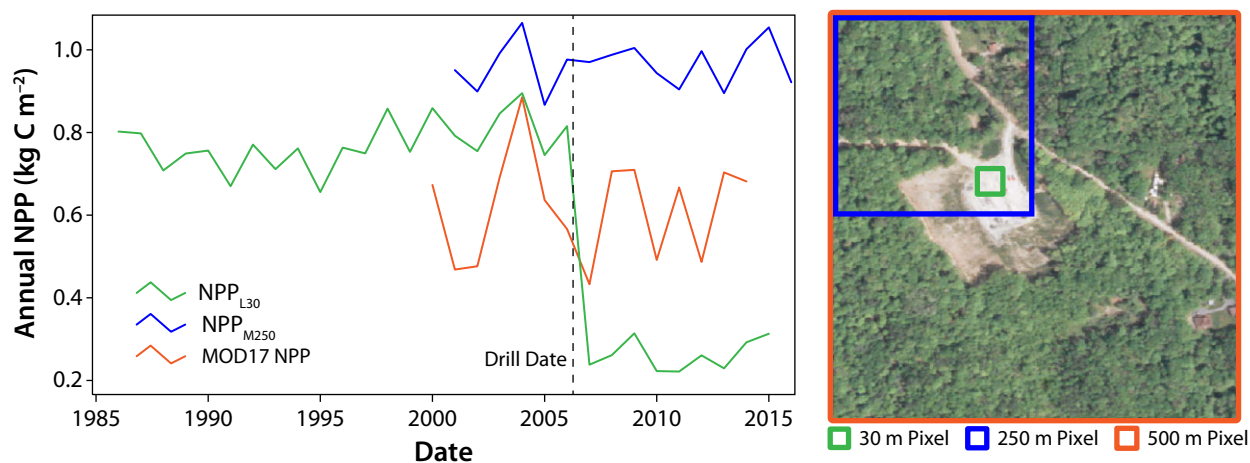


Figure 7. Annual NPP for an energy site using the MOD17 product (500 m), NPP_{M250} (250 m), and NPP_{L30} (30 m) datasets. The site was developed in 2006, and losses in NPP due to this discrete disturbance are reflected in the finer resolution NPP_{L30} dataset, but are absent in the coarser resolution datasets. The time series also highlights the historical data available using the full Landsat archive. The relative differences in pixel sizes are shown in the right panel. NPP, net primary production.

Emerging big data technologies and geospatial applications (e.g., Apache Spark, Google Earth Engine, etc.) enable new and dynamic approaches to geospatial product creation and distribution. A barrier to using Landsat or other fine resolution data is the access, retrieval, storage, and manipulation of images. As the spatiotemporal extents increase, so do data volume and compute processing needs, making it difficult or impractical to those without access to high performance computing facilities and the skills to work with such systems. We overcame these barriers and limitations by implementing the MOD17 algorithm in Google Earth Engine. The structure of Google Earth Engine creates the ability to incorporate data from multiple sensors and datasets to build even more robust products. What we accomplish with multiple Landsat sensors can be extended to include even higher resolution sensors, such as Sentinel-2. However, the real power of these new platforms and technologies is the ability to create customizable and dynamic geospatial products (Robinson et al. 2017). When algorithms are programmed into a web application, model parameters and input datasets can be customizable so that users not satisfied with the standard parameters or other inputs can modify them based on a priori knowledge. For example, a user working with a web application that utilizes the MOD17 algorithm to estimate productivity can correct misclassified pixels in land cover datasets, or select between standard approaches or fixed ratios to calculate respiration used in NPP. Models can be tuned for specific regions or environmental conditions, providing locally optimized products that are more appropriate for a given system or question.

The new Landsat (30 m; 1986 to 2016) and MODIS (250 m; 2001 to 2016) derived primary production products provide new opportunities in the study of production dynamics and variability. Of significance is the ability to utilize these datasets for conservation and management, as the scales of both the product and the conservation/management activities are now better aligned. These enhancements will advance the study of terrestrial primary production, enable future refinements, and generate new applications of vegetation productivity measures.

Acknowledgments

We thank the Google Earth Engine developers for their support and technical advice. This work was funded through a Google Earth Engine Research Award and by the NRCS Wildlife Conservation Effects Assessment Project and Sage Grouse Initiative. This work used eddy covariance data acquired and shared by the FLUXNET community, including these networks: AmeriFlux, AfriFlux, AsiaFlux, CarboAfrica, CarboEuropeIP, CarboItaly, CarboMont, ChinaFlux, Fluxnet-Canada, GreenGrass, ICOS, KoFlux, LBA, NECC, OzFlux-TERN, TCOS-Siberia, and USCCC. The ERA-Interim reanalysis data are provided by ECMWF and processed by LSCE. The FLUXNET eddy covariance data processing and harmonization was carried out by the European Fluxes Database Cluster, AmeriFlux Management Project, and Fluxdata project of FLUXNET, with the support of CDIAC and ICOS Ecosystem Thematic Center, and the OzFlux, ChinaFlux and AsiaFlux offices.

Conflict of Interest

The authors declare no conflict of interest.

References

- Abatzoglou, J. T. 2013. Development of gridded surface meteorological data for ecological applications and modelling. *Int. J. Climatol.* **33**, 121–131.
- Allred, B. W., W. K. Smith, D. Twidwell, J. H. Haggerty, S. W. Running, D. E. Naugle, et al. 2015. Ecosystem services lost to oil and gas in North America. *Science* **348**, 401–402.
- Byrd, R. H., P. Lu, J. Nocedal, and C. Zhu. 1995. A limited memory algorithm for bound constrained optimization. *SIAM J. Sci. Comput.* **16**, 1190–1208.
- Chen, T., G. R. van der Werf, A. J. Dolman, and M. Groenendijk. 2011. Evaluation of cropland maximum light use efficiency using eddy flux measurements in North America and Europe. *Geophys. Res. Lett.* **38**, L14707.
- Choudhury, B. J. 1987. Relationships between vegetation indices, radiation absorption, and net photosynthesis evaluated by a sensitivity analysis. *Remote Sens. Environ.* **22**, 209–233.
- Crabtree, R., C. Potter, R. Mullen, J. Sheldon, S. Huang, J. Harmsen, et al. 2009. A modeling and spatio-temporal analysis framework for monitoring environmental change using NPP as an ecosystem indicator. *Remote Sens. Environ.* **113**, 1486–1496.
- Cramer, W., D. W. Kicklighter, A. Bondeau, B. Moore III, G. Churika, B. Nemy, et al. 1999. Comparing global models of terrestrial net primary productivity (NPP): overview and key results. *Glob. Change Biol.* **5**, 1–15.
- DeLucia, E. H., J. E. Drake, R. B. Thomas, and M. Gonzalez-Meler. 2007. Forest carbon use efficiency: is respiration a constant fraction of gross primary production? *Glob. Change Biol.* **13**, 1157–1167.
- DeLucia, E. H., N. Gomez-Casanovas, J. A. Greenberg, T. W. Hudiburg, I. B. Kantola, S. P. Long, et al. 2014. The theoretical limit to plant productivity. *Environ. Sci. Technol.* **48**, 9471–9477.
- Feng, M., C. Huang, S. Channan, E. F. Vermote, J. G. Masek, and J. R. Townshend. 2012. Quality assessment of Landsat surface reflectance products using MODIS data. *Comput. Geosci.* **38**, 9–22.
- Field, C. B., J. T. Randerson, and C. M. Malmström. 1995. Global net primary production: Combining ecology and remote sensing. *Remote Sens. Environ.* **51**, 74–88.
- Fry, J. A., G. Xian, S. Jin, J. Dewitz, C.G. Homer, L. Yang, et al. 2011. Completion of the 2006 national land cover database for the conterminous United States. *Photogramm. Eng. Remote Sensing* **77**, 858–864.
- Gorelick, N., M. Hancher, M. Dixon, S. Ilyushchenko, D. Thau, and R. Moore. 2016. Google earth engine: planetary-scale geospatial analysis for everyone. *Remote Sens. Environ.* **202**, 18–27.
- Gunter, L., Y. Zhang, M. Jung, J. Joiner, M. Voigt, J. A. Berry, et al. 2014. Global and time-resolved monitoring of crop photosynthesis with chlorophyll fluorescence. *Proc. Natl Acad. Sci.* **111**, E1327–E1333.
- Haberl, H., N. B. Schulz, C. Plutzer, K. Heinz Erb, F. Krausmann, W. Loibl, et al. 2004. Human appropriation of net primary production and species diversity in agricultural landscapes. *Agr. Ecosyst. Environ.* **102**, 213–218.
- Haberl, H., K. H. Erb, F. Krausmann, V. Gaube, A. Bondeau, C. Plutzer, et al. 2007. Quantifying and mapping the human appropriation of net primary production in earth's terrestrial ecosystems. *Proc. Natl Acad. Sci. USA* **104**, 12942–12947.
- Hasenauer, H., R. Petritsch, M. Zhao, C. Boisvenue, and S. W. Running. 2012. Reconciling satellite with ground data to estimate forest productivity at national scales. *For. Ecol. Manage.* **276**, 196–208.
- Heinsch, F. A., M. Zhao, S. W. Running, J. S. Kimball, R. R. Nemani, K. J. Davis, et al. 2006. Evaluation of remote sensing based terrestrial productivity from MODIS using regional tower eddy flux network observations. *IEEE Trans. Geosci. Remote Sens.* **44**, 1908–1925.
- Homer, C., J. Dewitz, J. Fry, M. Coan, N. Hossain, C. Larsion, et al. 2007. Completion of the 2001 national land cover database for the conterminous United States. *Photogramm. Eng. Remote Sensing* **73**, 337.
- Homer, C. G., J. A. Dewitz, L. Yang, S. Jin, P. Danielson, G. Xian, et al. 2015. Completion of the 2011 National Land Cover Database for the conterminous United States—Representing a decade of land cover change information. *Photogramm. Eng. Remote Sensing* **81**, 345–354.
- Hunt, E. R., and B. A. Miyake. 2006. Comparison of stocking rates from remote sensing and geospatial data. *Rangeland Ecol. Manag.* **59**, 11–18.
- Julien, Y., and J. A. Sobrino. 2010. Comparison of cloud-reconstruction methods for time series of composite NDVI data. *Remote Sens. Environ.* **114**, 618–625.
- Keeling, H. C., and O. L. Phillips. 2007. The global relationship between forest productivity and biomass. *Glob. Ecol. Biogeogr.* **16**, 618–631.
- Madani, N., J. S. Kimball, D. L. R. Affleck, J. Kattage, J. Graham, P.M. van Bodegom, et al. 2014. Improving ecosystem productivity modeling through spatially explicit estimation of optimal light use efficiency. *J. Geophys. Res. Biogeosci.* **119**, 1755–1769.
- Masek, J. G., E. F. Vermote, N. E. Saleous, R. Wofle, F. G. Hall, K. F. Huemmrich, et al. 2006. A landsat surface reflectance dataset for North America, 1990–2000. *IEEE Geosci. Remote Sens. Lett.* **3**, 68–72.
- McDonald, R. I., J. Fargione, J. Kiesecker, W. M. Miller, and J. Powell. 2009. Energy sprawl or energy efficiency: climate

- policy impacts on natural habitat for the United States of America. *PLoS ONE* **4**, e6802.
- McGuire, A. D., S. Sitch, J. S. Clein, G. Esser, J. Foley, M. Heimann, et al. 2001. Carbon balance of the terrestrial biosphere in the twentieth century: analyses of CO₂, climate and land use effects with four process-based ecosystem models. *Global Biogeochem. Cycles* **15**, 183–206.
- Monfreda, C., N. Ramankutty, and J. A. Foley. 2008. Farming the planet: 2. Geographic distribution of crop areas, yields, physiological types, and net primary production in the year 2000. *Global Biogeochem. Cycles* **22**: GB1022.
- Monteith, J. L. 1972. Solar radiation and productivity in tropical ecosystems. *J. Appl. Ecol.* **9**, 747–766.
- Neumann, M., A. Moreno, C. Thurnher, V. Mues, S. Härkönen, M. Mura, et al. 2016. Creating a regional MODIS satellite-driven net primary production dataset for European forests. *Remote Sens.* **8**, 554.
- Peng, D., B. Zhang, and L. Liu. 2012. Comparing spatiotemporal patterns in Eurasian FPAR derived from two NDVI-based methods. *Int. J. Digital Earth* **5**, 283–298.
- Piao, S., P. Ciais, P. Friedlingstein, deNoblet-Ducoudré N., P. Cadule, N. Viovy, et al. 2009. Spatiotemporal patterns of terrestrial carbon cycle during the 20th century. *Global Biogeochem. Cycles*, **23**, GB4026.
- Reeves, M. C., M. Zhao, and S. W. Running. 2006. Applying improved estimates of MODIS productivity to characterize grassland vegetation dynamics. *Rangeland Ecol. Manag.* **59**, 1–10.
- Richardson, A. D., T. A. Black, P. Ciais, N. Delbart, M. A. Friedl, N. Gobron, et al. 2010. Influence of spring and autumn phenological transitions on forest ecosystem productivity. *Philos. Trans. R. Soc. Lond. B Biol. Sci.* **365**, 3227–3246.
- Robinson, N. P., B. W. Allred, M. O. Jones, A. Moreno, J. S. Kimball, D. E. Naugle, et al. 2017. A dynamic Landsat derived normalized difference vegetation index (NDVI) product for the conterminous United States. *Remote Sens.* **9**, 863.
- Ruimy, A., B. Saugier, and G. Dedieu. 1994. Methodology for the estimation of terrestrial net primary production from remotely sensed data. *J. Geophys. Res.* **99**, 5263–5283.
- Running, S. W. 2012. Ecology. A measurable planetary boundary for the biosphere. *Science* **337**, 1458–1459.
- Running, S. W., and M. Zhao. 2015. *MOD17 Users Guide 2015*. Numerical Terra Dynamic Simulation Group,000.
- Running, S.W., P.E. Thornton, R. Nemani, J. M. Glassy. 2000. Global terrestrial gross and net primary productivity from the earth observing system Pp. 44–57 in O. E. Sala, et al. *Methods in Ecosystem Science*. Springer, New York.
- Running, S. W., R. R. Nemani, F. A. Heinsch, M. Zhao, M. Reeves, and H. Hashimoto. 2004. A continuous satellite-derived measure of global terrestrial primary production. *Bioscience* **54**, 547–560.
- Santaren, D., P. Peylin, N. Viovy, and P. Ciais. 2007. Optimizing a process-based ecosystem model with eddy-covariance flux measurements: a pine forest in southern France. *Global Biogeochem. Cycles*. **21**, GB2013.
- Scurlock, J. M. O., W. Cramer, R. J. Olson, W. J. Parton, and S. D. Prince. 1999. Terrestrial NPP: toward a consistent data set for global model evaluation. *Ecol. Appl.* **9**, 913–919.
- Sellers, P. J., C. J. Tucker, G. J. Collatz, S. O. Los, C. O. Justice, D. A. Dazlich, et al. 1994. A global 1° by 1° NDVI data set for climate studies. Part 2: the generation of global fields of terrestrial biophysical parameters from the NDVI. *Int. J. Remote Sens.* **15**, 3519–3545.
- Serrano-Ortiz, P., C. Oyonarte, O. Pérez-Priego, B. R. Reverter, E. P. Sánchez-Cañete, A. Were, et al. 2014. Ecological functioning in grass–shrub Mediterranean ecosystems measured by eddy covariance. *Oecologia* **175**, 1005–1017.
- Sims, D. A., A. F. Rahman, V. D. Cordova, B. Baldocchi, P. Bolstad, L. Flanagan, et al. 2008. A new model of gross primary productivity for North American ecosystems based solely on the enhanced vegetation index and land surface temperature from MODIS. *Remote Sens. Environ.* **112**, 1633–1646.
- Smith, W. K., M. Zhao, and S. W. Running. 2012a. Global bioenergy capacity as constrained by observed biospheric productivity rates. *Bioscience* **62**, 911–922.
- Smith, W. K., C. C. Cleveland, S. C. Reed, N. L. Miller, and S. W. Running. 2012b. Bioenergy potential of the United States constrained by satellite observations of existing productivity. *Environ. Sci. Technol.* **46**, 3536–3544.
- Smith, W. K., S. C. Reed, C. C. Cleveland, A. P. Ballantyne, W. R. L. Anderegg, W. R. Wieder, et al. 2016. Large divergence of satellite and Earth system model estimates of global terrestrial CO₂ fertilization. *Nat. Clim. Chang.* **6**, 306–312.
- Trainor, A. M., R. I. McDonald, and J. Fargione. 2016. Energy sprawl is the largest driver of land use change in United States. *PLoS ONE* **11**, e0162269.
- Turner, D. P., W. D. Ritts, W. B. Cohen, S. T. Gower, M. Zhao, S. W. Running, et al. 2003. Scaling gross primary production (GPP) over boreal and deciduous forest landscapes in support of MODIS GPP product validation. *Remote Sens. Environ.* **88**, 256–270.
- Turner, D. P., S. V. Ollinger, and J. S. Kimball. 2004. Integrating remote sensing and ecosystem process models for landscape- to regional-scale analysis of the carbon cycle. *Bioscience* **54**, 573–584.
- Turner, D. P., W. D. Ritts, W. B. Cohen, T. K. Maeirsperger, S. T. Gower, A. A. Kirschbaum, et al. 2005. Site-level evaluation of satellite-based global terrestrial gross primary production and net primary production monitoring. *Glob. Change Biol.* **11**, 666–684.
- Turner, D. P., W. D. Ritts, J. M. Styles, Z. Yang, W. B. Cohen, B. E. Law, et al. 2006. A diagnostic carbon flux model to monitor the effects of disturbance and interannual variation

- in climate on regional NEP. *Tellus. B Chem. Phys. Meteorol.* **58**, 476–490.
- Turner, D. P., W. D. Ritts, S. Wharton, C. Thomas, R. Monson, T. A. Black, et al. 2009. Assessing FPAR source and parameter optimization scheme in application of a diagnostic carbon flux model. *Remote Sens. Environ.* **113**, 1529–1539.
- Van Oijen, M., A. Schapendonk, and M. Höglind. 2010. On the relative magnitudes of photosynthesis, respiration, growth and carbon storage in vegetation. *Ann. Bot.* **105**, 793–797.
- Verma, M., M. A. Friedl, B. E. Law, D. Bonal, G. Kiely, T. A. Black, et al. 2015. Improving the performance of remote sensing models for capturing intra- and inter-annual variations in daily GPP: An analysis using global FLUXNET tower data. *Agric. For. Meteorol.* **214–215**, 416–429.
- Vermote, E. 2015. MOD09 (006) [Data set]. <https://doi.org/10.5067/modis/mod09q1.006>
- Vermote, E., C. Justice, M. Claverie, and B. Franch. 2016. Preliminary analysis of the performance of the Landsat 8/OLI land surface reflectance product. *Remote Sens. Environ.* **185**, 46–56.
- Vitousek, P. M., P. R. Ehrlich, A. H. Ehrlich, and P. A. Matson. 1986. Human appropriation of the products of photosynthesis. *Bioscience* **36**, 368–373.
- Wang, J., J. Dong, J. Liu, M. Hauang, G. Li, S. Running, et al. 2014. Comparison of gross primary productivity derived from GIMMS NDVI3 g, GIMMS, and MODIS in Southeast Asia. *Remote Sens.* **6**, 2108–2133.
- Wood, J. D., T. J. Griffis, J. M. Baker, C. Frankenberg, M. Verma, and K. Yuen. 2017. Multiscale analyses of solar-induced fluorescence and gross primary production. *Geophys. Res. Lett.* **44**, 533–541.
- Yang, Y., Q. Zhu, C. Peng, H. Wang, and H. Chen. 2015. From plant functional types to plant functional traits: a new paradigm in modelling global vegetation dynamics. *Prog. Phys. Geogr.* **39**, 514–535.
- Zhang, Y., M. Xu, H. Chen, and J. Adams. 2009. Global pattern of NPP to GPP ratio derived from MODIS data: effects of ecosystem type, geographical location and climate. *Glob. Ecol. Biogeogr.* **18**, 280–290.
- Zhao, M., F. A. Heinsch, R. R. Nemani, and S. W. Running. 2005. Improvements of the MODIS terrestrial gross and net primary production global data set. *Remote Sens. Environ.* **95**, 164–176.

Supporting Information

Additional supporting information may be found online in the supporting information tab for this article.

Data S1. Methods.

Figure S1. Illustration of the linear ramp functions for scaling minimum temperature and vapor pressure deficit.

Figure S2. Map of individual flux tower sites used for the GPP parameter optimization. The numbers correspond with individual flux towers described in Table S1.

Figure S3. (A) The NLCD within a 1 km buffer of the Wi4 flux tower located in Northern Wisconsin, demonstrating heterogeneous land cover cover at 30 m resolution.

Figure S4. Boxplots showing pre- and post-fire NPP dynamics (anomalies) relative to burn severity for a grassland fire (top panels; Lund fire, North Dakota) and an evergreen needleleaf forest fire (bottom panels; Horse Creek fire, Wyoming) using the MOD17 (500 m), NPP_{M250} (250 m), and NPP_{L30} (30 m) products.

Figure S5. The GPP/NPP_{L30} datasets permit the tracking of primary production change across broad spatiotemporal scales. Here, annual NPP for a 60 m buffer around Maggie Creek, Nevada is plotted. Restoration activities occurred in 1994 (vertical black line).

Figure S6. Time series of NPP anomalies including the MODIS and Landsat derived NPP calculated with respiration as a fixed ratio (50%) of GPP.

Table S1. Flux Tower Info.

Table S2. Total annual NPP for CONUS in Pg (10^{15} g) carbon for MOD17, NPP_{M250} and NPP_{L30} calculated with respiration as a fixed ratio of GPP and with the MOD17 procedure.

Table S3. Biome specific properties used in the MOD17 algorithm (Running & Zhao, 2015).

Table S4. Reclassification scheme for National Land Cover Database (NLCD). Grassland and pasture/hay are combined as grassland.